Development of a Fast-Charging Platform for Buried Sensors Using High Frequency IPT for Agricultural Applications

Juan M. Arteaga, Paul D. Mitcheson and Eric M. Yeatman
Department of Electrical and Electronic Engineering, Imperial College London
j.arteaga-saenz15@imperial.ac.uk

***Abstract*—This paper describes the methodology and experimental results for wireless power delivery to a soil-sensors power and data distribution unit from an unmanned aerial vehicle (UAV), using a high frequency inductive power transfer (HF-IPT) link. The configuration features, at the transmit side, a lightweight single-turn air-core coil driven by a 13.56 MHz Class EF inverter mounted on a Matrice 100 drone by DJI, and at the receive side, a two-turn PCB coil with a voltage-tipler Class D rectifier, an off-the-shelf 42 V battery charger and a supercapacitors module for energy storage. The experiments were conducted with a coil-to-coil gap of 250 mm, which corresponds to a coupling factor lower than 5%. In the experiments, a 10 F, 42 V supercapacitors module was charged in eleven minutes with an energy efficiency of 34% from the 80 V DC source that feeds the inverter on the drone to the supercapacitor-based energy storage unit in the sensor module. At higher power (50 W) the HF-IPT system was able to achieve a 68% DC-DC efficiency with a coupling factor of 3.5%.**

The work reported in this paper is part of a multiple-discipline project which looks to enable the optimal usage of water in agriculture with broader sensing techniques and more frequent sensing cycles.

I. Introduction

Real-time monitoring of the physical and chemical parameters of the soil in agricultural fields allows more effective irrigation strategies to be conducted for effective farming and to keep the soil healthy. Irrigation strategies depend on location, weather and types of crops, and the optimisation of such strategies heavily rely on measurements and models of the condition of the soil [1]. This work proposes enabling higher availability of energy to the agricultural soil sensors by periodically providing power, wirelessly, through a high-frequency inductive power transfer (HF-IPT) link, to therefore unlock more energy-demanding strategies of sensing.

The progression and uptake of inductive power transfer (IPT) technology has been substantial since it was introduced in industrial applications in the 1990s [2]. It has been demonstrated in multiple forms and for an extensive number of applications, ranging from electric vehicles to sensors in locations difficult to access [3]–[8]. Inductive charging is now a common feature in mobile phones and other low power, small airgap applications.

With the introduction of more capable switching devices, IPT has been pushed further not only in terms of power but also in terms of operating frequency. Fundamentally, the advantage of operating at higher frequencies is the reduction of the required inductance of the transmit and receive coils. In the MHz range, the coils tend to be constructed with a low number of turns (usually less than ten) and they tend to not employ ferromagnetic materials, other than for shielding. HF-IPT systems, which operate at the first ISM bands (6.78 MHz, 13.56 MHz, 27.12 MHz), have been demonstrated in sub-kilowatt applications achieving high efficiencies (in cases higher than 90 %), with other advantageous features such as large airgaps and extensive tolerance to misalignment [9]–[11].

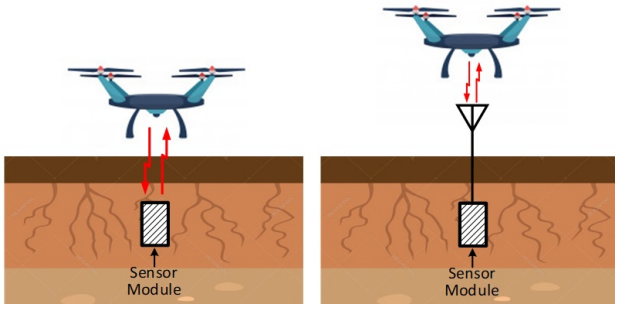

Fig. 1. Power delivery diagram.

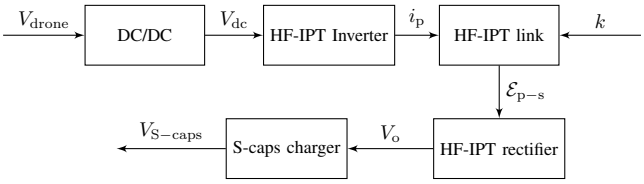

Fig. 2. Drone to sensor-module power-delivery block diagram.

II. Design of a HF-IPT System for Agricultural Sensors in the Soil

Fig. 1 illustrates the proposed power delivery strategy for agricultural sensors buried in the field. The UAV is used to feed energy and recover data from a module which feeds power and stores data from a cluster of sensors in the soil. The concept of power delivery using a HF-IPT link, and concurrently gathering data using drones was first introduced in our previous work [12].

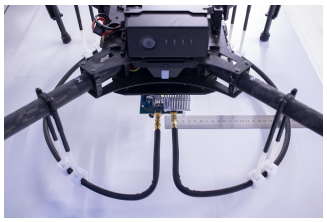

(a) Transmit coil

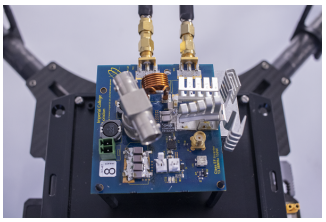

(b) HF-IPT inverter board

Fig. 3. Photographs of the HF-IPT transmitter on the Matrice 100 drone.

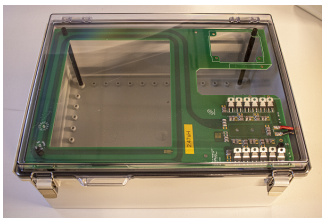

(a) Coil and rectifier PCB

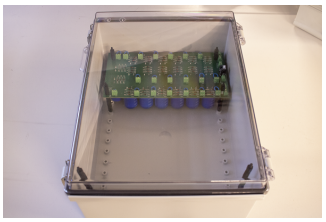

(b) Energy storage module

Fig. 4. Photographs of the receiver enclosure.

The power delivery is proposed to be conducted as shown in the block diagram in Fig. 2. The battery on the drone is accounted as the primary source of power. The voltage which it provides has to be transformed into the voltage required by the inverter with a DC-DC converter. The HF-IPT inverter then feeds high frequency current (i_{p}) to the coil to induce a voltage on the receiving coil ($\mathcal{E}_{\mathrm{p-s}}$) which then feeds a battery or supercapacitors module charger circuit until the unit is fully charged.

A. Design Considerations of the End-to-end System

The realisation of the proposed energy delivery strategy was designed with a Matrice 100 quadcopter by DJI at the transmit side and a plastic enclosure with IP67 rating (with the following internal dimensions: length: 370 mm, width: 270 mm, height: 150 mm) at the receive side. This enclosure was selected to withstand being buried in the agricultural field.

Considering these application-specific bounds, the HF IPT system was designed to operate using a single-turn 10 mm diameter 0.9 mm wall-thickness copper-pipe coil at the transmit side with a 200 mm radius (Fig. 3(a), which is similar to a previously proven HF-IPT coil on a Matrice 100 drone [13]) to minimise the impact of the wireless charging system on the airflow of the drone, and a receiver with a rectangular two-turn PCB coil (with external dimensions of 250 mm by 200 mm, Fig. 4(a)), dictated by the dimension restrictions of the enclosure.

The operating frequency was selected to be 13.56 MHz, which is the optimal ISM band for the inductance of these coils (specified in Tables I and II).

We are currently investigating the effects of a soil layer between the coils, which might differ with different soil samples, however early experiments show that this layer does not heavily load or detune the link, as long as the soil is not in direct contact with the traces of the coil. These experiments are described in Section III-A.

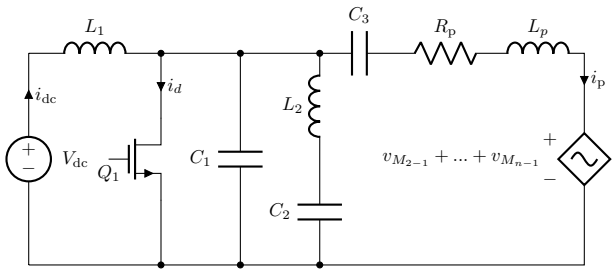

Fig. 5. Circuit topology of a single-ended Class EF inverter.

TABLE I
COMPONENT VALUES FOR THE INVERTER

Component	Value	Description
C_1 (pF)	156+C_{oss}	TDK C Series
C_2 (pF)	200	TDK C Series
C_3 (pF)	140	TDK C Series
L_1 (μH)	88	TDK C Series
L_2 (nH)	251	Coilcraft 2014VS
L_{p} (nH)	1181	Copper-pipe coil
Q_1	GS66504B (650 V, 15 A) GaN FET	

B. Design of the Transmit Side

The HF-IPT transmitter was mounted on a Matrice 100 drone using plastic fixtures (Fig. 3(a)). The coil was fastened at the bottom of the drone to achieve a ground clearance of 15 mm.

The drone's battery (TB47D by DJI) has a capacity of 4500 mA h and a nominal voltage of 22.2 V. Energy from this battery can be accessed using the XC60 or XC30 reserved ports, which output the battery's voltage and a maximum current of 10 A. With the addition of an in-house variable-output DC-DC converter which boosts up the voltage to the typical input voltages of these coil drivers (usually from 60 V to 150 V), we managed to drive the inverter using the drone's battery as a primary source of energy; however, the results reported in this paper were conducted with a power supply at 80 V next to the drone.

The inverter was designed following the guidelines in [14], which allows driving the transmit coil with load-independent current amplitude and phase. The inverter in this design drives the coil with a peak current of 6.25 A. The topology of the Class EF inverter is illustrated in Fig. 5, and the values and the component details are specified in Table I. The inverter was tuned considering the metallic structure of the drone. Fig. 3(b) shows a photograph of the inverter board.

C. Design of the Receive Side

The receive side uses a voltage tripler Class D rectifier [15], to maximise the induced-voltage-to-output-voltage gain of the

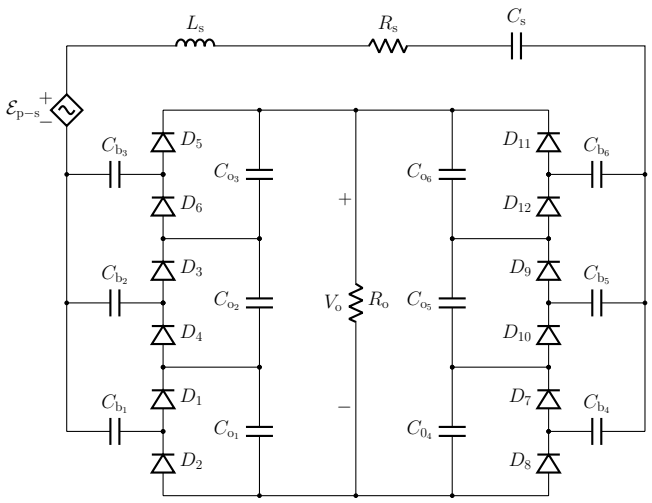

Fig. 6. Circuit topology of a voltage-tripler full-wave Class D rectifier for high output voltage.

TABLE II
COMPONENT VALUES FOR THE RECTIFIER

Component	Value	Description
C_s (pF)	58.5	TDK C Series
C_{o_1}-C_{o_6}, C_{b_1}-C_{b_6} (nF)	200	TDK C Series
L_s (nH)	2470	Copper-pipe coil
$D_1 - D_{12}$	Vishay MBRF10100 (100 V, 10 A) Schottky diodes	

rectifier. This topology was selected with two purposes. First, to employ an off-the-shelf battery charger as the next power conversion stage which requires an input voltage from 95 V to 240 V; and second, to increase the sensitivity of an IPT-based sensor localisation mechanism, which can be then included in the navigation system of the drone [16]. The topology of the rectifier, which has been employed in this type of system [17], can be found in Fig. 6 and the component values are presented in Table II. The behaviour of the rectifier differs slightly from the one expected from theory because at this frequency the parasitics of the board (which are inevitable with the available diode packages), and the junction capacitance of the diodes cannot be neglected. The divergence of the experimental input impedance from the theoretical one in non-synchronous Class E and Class D rectifiers (including the voltage-tripler) has been investigated at 13.56 MHz in [18], with results from large-signal experiments.

After the rectifier, an off-the-shelf 2 A, 42 V battery charger was used to feed a module of twenty 200 F supercapacitors (SSC-Series by AVX) in series. The battery charger was modified to output a constant current of 350 mA rather than 2 A as a precaution not to overload the transmit side, which will be ultimately powered by the battery of the drone.

Fig. 7. Photograph of the end-to-end HF-IPT experimental setup.

III. EXPERIMENTAL RESULTS

In order to test the HF-IPT link, an experimental setup was assembled (Fig. 7). The drone's battery coupled with an in-house light-weight boost converter as the source of power (which has been tested) was emulated with a bench power supply for testing and direct control on the inverter's input voltage at the time of the experiments. A white perspex structure, shown in the photograph in Fig. 7 allows the drone to be placed at different positions and to evaluate the system at different coil alignments which is a situation to be expected without a precision landing system and a precise sensor module localisation system on the drone.

A. Testing the HF-IPT System

The coil separation was established at 250 mm, which is the point in which the designed coupling range (3 % to 5 %) is achieved, with a lateral alignment tolerance of one receive-coil radius in any direction. At concentric alignment, the coupling was measured at 4.9 %. Coupling measurements were conducted using a Keysight E4990A impedance analyser. Once the inverter was switched on, the voltage at the output of the rectifier was recorded at 179 V when loaded, and roughly a 5 % increase in the output voltage is observed when the system becomes unloaded. Throughout the experiments, the relative position of the coils was changed to achieve a coupling factor from 3.1 % to 4.9 %. Notwithstanding that these measurements were conducted with a wireless airgap, it is expected that the enclosure should withstand to be buried with a 150 mm depth (plus the airgaps between the transmit coil and ground, and the receive coil and the lid of the enclosure) and achieve similar results.

DC to DC experiments were conducted at a 3.5 % coupling with soil samples close to the transmit and receive coils respectively (Fig. 8). During the experiments, the performance was not heavily compromised as shown in Table III, where the results of the DC-to-DC HF-IPT experiments are summarised.

Fig. 9 shows the drain voltage waveforms of the Class EF inverter, from which it is possible to determine the induced voltage from coupled objects, those being a receiver which loads the inverter, or a medium which causes detuning [19],

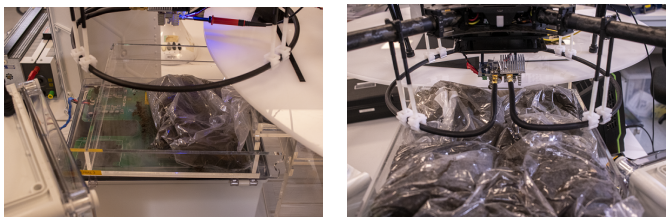

(a) Close to the receiver (b) Close to the transmitter

Fig. 8. Photographs of the HF-IPT system operating with soil samples close to the coils.

TABLE III
RESULTS FROM THE HF-IPT EXPERIMENTS

Experiment	P_{i} [W]	V_{o} [V]	I_{o} [A]	$\eta_{\mathrm{DC-DC}}$
No-Load	24.8			
DC-DC	75.2	155.0	0.33	68.0 %
DC (soil)-DC	78.4	157.1	0.32	64.1 %
DC-DC (soil)	78.4	158.8	0.33	66.8 %

[20]. As can be appreciated by the trajectory of the waveforms with and without the soil samples, the induced voltage (or the total reflected impedance) only caused a small divergence in the equivalent self and mutual inductance of the coils, which slightly affects the tuning and coupling, and hence the power throughput and the efficiency.

B. Testing the Energy Storage System

As an energy storage system, a module of supercapacitors was designed and assembled to allow for fast charging, which is required by the application. The in-house energy storage board (Fig.3(b)) employs twenty SSC-Series 200 F supercapacitors by AVX in series, each with Zener diodes in parallel to prevent voltage imbalances between the supercapacitors. The size of this module was designed to fit the enclosure (length: 255 mm, width: 130 mm, height: 80 mm). Throughout the experiments, the voltage of the module was evenly distributed between the supercapacitors and no significant dissipation of power was recorded in the Zener diodes with the thermal camera (a Fluke Ti400).

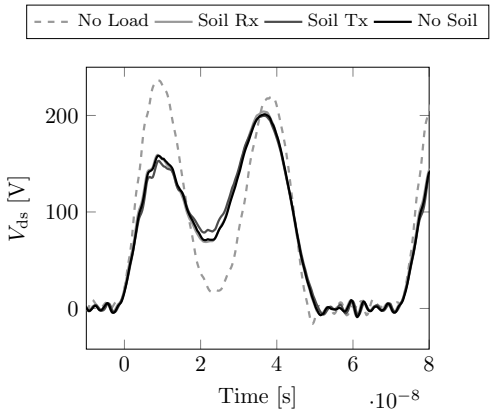

Fig. 9. Experimental waveforms of the drain voltage of the transistor in the Class EF inverter.

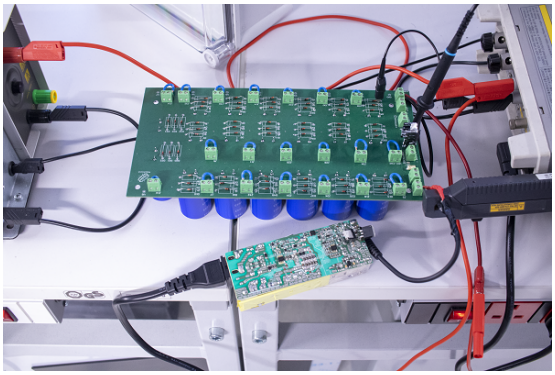

Fig. 10. Experimental setup for charge and discharge of the supercapacitors module.

As an intermediate power conversion stage, an off-the-shelf 42 V, 2 A constant-current, constant-voltage charger was employed to drive the supercapacitors module from the output of the rectifier. This board was modified to output 350 mA instead of 2 A as a conservative precaution, not to overload the battery of the drone at any point of charging in the trial of the application.

The first tests on this module were conducted by plugging the charger to the mains and charge the supercapacitors module in parallel with a rheostat (1125 Ω), which would then be used to discharge the supercapacitors. Fig. 10 shows a photograph of the setup. The experimental results are summarised in the plots in Fig. 11, where the voltage of the supercapacitors module and the current of the charger were measured using an oscilloscope (Teledyne LeCroy HDO4104) with a 500 s time window and the trigger set at 40 V for the voltage in the supercapacitors module.

All the experiments involving the supercapacitors module were made with a 20 V minimum voltage due to the charger having an under-voltage protection system where the charging under this point is done with pulses rather than constant current. The charger does bring the voltage of the supercapacitors module up to 42 V from zero, but under 20 V, it is done at a much slower rate. This is not a concern for the application at hand because the voltage in the supercapacitors module is not expected to decrease beyond this point, considering the energy available for the sensors in between energy delivery missions of the drone.

C. Charging the Supercapacitors Module from the Drone with a 250 mm Wireless Gap

Finally, the drone-to-supercapacitors-module end-to-end system was assembled (Fig. 12) with the addition of a DC-DC converter to feed a micro-controller and a Bluetooth module to monitor the rectifier parameters once the sensor module is

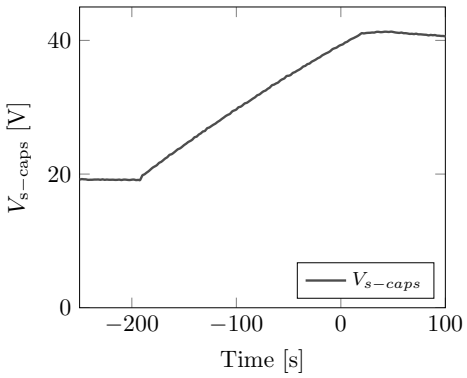

(a) Supercapacitors module voltage

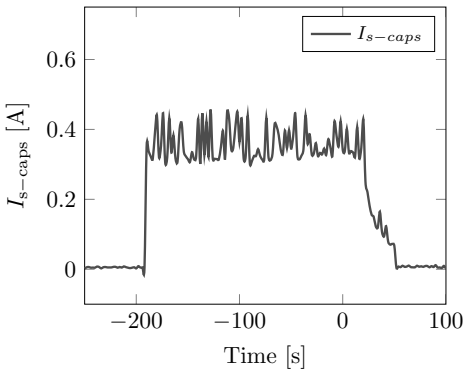

(b) Charger current

Fig. 11. Experimental results from the standalone supercapacitor module charging experiment.

Fig. 12. Photograph of the drone to supercapacitors module end-to-end experiment in operation.

buried in the field. The results of the experiments are summarised in Fig. 13. The voltage of the supercapacitors module was monitored with a power meter (WT210 by Yokogawa) and readings of the variables of the system were recorded when the voltage of the supercapacitors module increased by 1 V. The output power was calculated from these readings and the expected output current of the charger (based on previous experiments) since the current probe does not fit

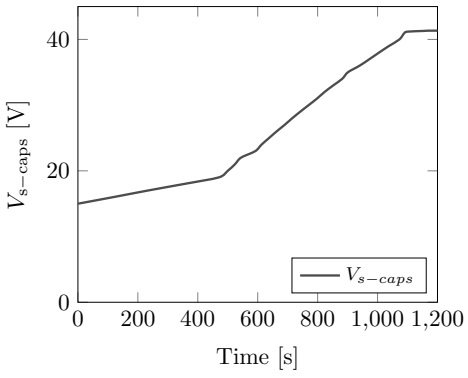

(a) Supercapacitors module voltage

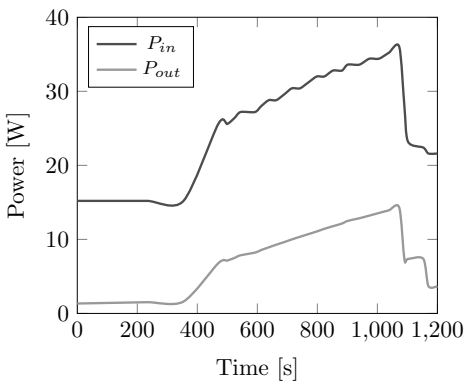

(b) Input and output power

Fig. 13. Plots of the voltage of the supercapacitors module, the HF-IPT system input power and the battery charger output power once the charging process started.

in the enclosure. Therefore, the power consumption of the additional boards is taken into account as part of the output power, which is why the charging time in these experiments increased from the previous ones.

The initial voltage of the supercapacitors module was set at 15 V to verify that the transmit side can withstand the low-voltage operation mode of the charger. Once it reached 20 V, the rate of charge drastically increased, and after eleven minutes the maximum voltage was achieved. The total energy-efficiency from the drone to the supercapacitors module charging from 20 V to 40 V was calculated at 34 %, with a peak power efficiency of 40 % shortly before the 42 V threshold was reached. These initial results are expected to be significantly outperformed in the field experiments which will be carried out at higher power (with higher current in the supercapacitor module charger). The power throughput and efficiency results in the HF-IPT experiments of Section III-A, and the efficiencies recorded on the other power modules operating individually suggest that at higher power (around 50 W at the output), the end-to-end energy efficiency can be significantly increased.

IV. Conclusion and Future Work

This paper covers the design methodology and the description of the experiments which validate a HF-IPT system as candidate for wireless power transfer to energise a power distribution unit for agricultural sensors in the soil.

Future work will look at increasing the power throughput, which is expected to increase the energy efficiency and accelerate the charging process. A first field trial of this concept is scheduled for February 2022.

Acknowledgement

The authors would like to acknowledge the following funding sources: SitS NSF-UKRI: Wireless In-Situ Soil Sensing Network for Future Sustainable Agriculture'.

References

[1] E. Vories and K. Sudduth, "Determining sensor-based field capacity for irrigation scheduling," *Agricultural Water Management*, vol. 250, p. 106860, 2021.

[2] G. A. Covic and J. T. Boys, "Inductive power transfer," *Proceedings of the IEEE*, vol. 101, no. 6, pp. 1276–1289, 2013.

[3] K. Van Schuylenbergh and R. Puers, *Inductive powering: Basic theory and application to biomedical systems*. Springer Science & Business Media, 2009.

[4] G. Covic, J. T. Boys *et al.*, "Modern trends in inductive power transfer for transportation applications," *IEEE Trans. Emerg. Sel. Topics Power Electron.*, vol. 1, no. 1, pp. 28–41, 2013.

[5] S. Y. R. Hui, W. Zhong, and C. K. Lee, "A critical review of recent progress in mid-range wireless power transfer," *IEEE Trans. on Power Electron.*, vol. 29, no. 9, pp. 4500–4511, Sept 2014.

[6] R. Bosshard, J. W. Kolar, J. Mühlethaler, I. Stevanović, B. Wunsch, and F. Canales, "Modeling and η - α -pareto optimization of inductive power transfer coils for electric vehicles," *IEEE Trans. Emerg. Sel. Topics Power Electron.*, vol. 3, no. 1, pp. 50–64, March 2015.

[7] J. M. Arteaga, S. Aldhaher, G. Kkelis, C. Kwan, D. C. Yates, and P. D. Mitcheson, "Dynamic capabilities of multi-MHz inductive power transfer systems demonstrated with batteryless drones," *IEEE Trans. on Power Electron.*, vol. 34, no. 6, pp. 5093–5104, June 2019.

[8] C. H. Kwan, J. M. Arteaga, D. C. Yates, and P. D. Mitcheson, "Design and construction of a 100 W wireless charger for an e-scooter at 6.78 MHz," in *IEEE PELS Workshop on Emerging Technologies: Wireless Power Transfer (WoW)*, 2019, pp. 186–190.

[9] A. L. F. Stein, P. A. Kyaw, and C. R. Sullivan, "Wireless power transfer utilizing a high-q self-resonant structure," *IEEE Trans. on Power Electron.*, vol. 34, no. 7, pp. 6722–6735, 2019.

[10] G. Zulauf and J. M. Rivas Davila, "Single-turn air-core coils for high-frequency inductive wireless power transfer," *IEEE Trans. on Power Electron.*, pp. 1–1, 2019.

[11] J. M. Arteaga, S. Aldhaher, G. Kkelis, D. C. Yates, and P. D. Mitcheson, "Multi-MHz IPT systems for variable coupling," *IEEE Trans. on Power Electron.*, vol. 33, no. 9, pp. 7744–7758, Sept 2018.

[12] P. D. Mitcheson, D. Boyle, G. Kkelis, D. Yates, J. M. Arteaga, S. Aldhaher, and E. Yeatman, "Energy-autonomous sensing systems using drones," in *2017 IEEE SENSORS*, Oct 2017, pp. 1–3.

[13] L. Lan, C. H. Kwan, J. M. Arteaga, D. C. Yates, and P. D. Mitcheson, "A 100 W 6.78 MHz inductive power transfer system for drones," in *European Conference on Antennas and Propagation (EuCAP)*, 2020, pp. 1–4.

[14] S. Aldhaher, D. C. Yates, and P. D. Mitcheson, "Load-independent class E/EF inverters and rectifiers for MHz-switching applications," *IEEE Trans. on Power Electron.*, pp. 1–1, 2018.

[15] M. M. Weiner, "Analysis of cockcroft-walton voltage multipliers with an arbitrary number of stages," *Review of Scientific Instruments*, vol. 40, no. 2, pp. 330–333, 1969.

[16] L. Lan, T. Polonelli, Y. Qin, N. Pucci, C. H. Kwan, J. M. Arteaga, D. Boyle, D. C. Yates, E. M. Yeatman, and P. D. Mitcheson, "An induction-based localisation technique for wirelessly charged drones," in *2020 IEEE PELS Workshop on Emerging Technologies: Wireless Power Transfer (WoW)*, 2020, pp. 275–277.

[17] J. M. Arteaga, S. Aldhaher, D. C. Yates, and P. D. Mitcheson, "A multi-MHz wireless power transfer system with mains power factor correction circuitry on the receiver," in *IEEE Applied Power Electron. Conf.*, March 2019, pp. 1–6.

[18] J. M. Arteaga, L. Lan, C. H. Kwan, D. C. Yates, and P. D. Mitcheson, "Characterisation of high frequency inductive power transfer receivers using pattern recognition on the transmit side waveforms," in *2020 IEEE Applied Power Electronics Conference and Exposition (APEC)*, 2020, pp. 825–831.

[19] J. M. Arteaga, N. Pucci, L. Lan, and P. D. Mitcheson, "Load characterization in high-frequency ipt systems using class ef switching waveforms," *IEEE Transactions on Power Electronics*, vol. 36, no. 10, pp. 11 036–11 044, 2021.

[20] N. Pucci, J. M. Arteaga, C. Kwan, D. C. Yates, and P. D. Mitcheson, "Induced voltage estimation from class ef switching harmonics in hf-ipt systems," *IEEE Transactions on Power Electronics*, pp. 1–1, 2021.